Multimodal Image Segmentation of Cellular Fragmentation Using Edge Detector and Morphological Operators

Article *in* Biomedizinische Technik/Biomedical Engineering · October 2014

CITATIONS
0

READS
65

6 authors, including:

Arif ul Maula Khan
Universität Heidelberg
16 PUBLICATIONS **16** CITATIONS
SEE PROFILE

Carsten Weiss
Karlsruhe Institute of Technology
144 PUBLICATIONS **2,111** CITATIONS
SEE PROFILE

Ralf Mikut
Karlsruhe Institute of Technology
237 PUBLICATIONS **1,406** CITATIONS
SEE PROFILE

Markus Reischl
Karlsruhe Institute of Technology
146 PUBLICATIONS **1,061** CITATIONS
SEE PROFILE

Multimodal Image Segmentation of Cellular Fragmentation Using Edge Detector and Morphological Operators

A. Khan[1], C. Weiss[2], B. Schweitzer[2], I. Hansjosten[2], R. Mikut[1] and M. Reischl[1]

[1]Institute for Applied Computer Science, Karlsruhe Institute of Technology, Germany

[2]Institute of Toxicology and Genetics, Karlsruhe Institute of Technology, Germany

Abstract

Image processing and analysis pipelines can be adapted to solve challenging biological cell segmentation problems. Occasionally, the image segmentation outcomes of images containing cells are unsatisfactory and insufficient if done alone in a single channel e.g. when staining the nucleus. An efficient method using morphological operators and edge detectors using information from an additional bright field (BF) channel is able to assign conflicting cases when segments of nuclei belonging to a single cell are detected artificially as independent objects by nuclear staining. This method is shown to improve the image segmentation accuracy of cell segmentation using the information from multiple channels in comparison to only using nuclear staining.

1 Introduction

Currently, the focus on using image processing techniques and methods in order to develop adequate comprehension of biological processes has become downright attractive, both to cell biologists and toxicologists. In multicellular organisms, different forms of cell death (such as apoptosis) are of lasting significance for various diseases such as cancer. Image data sets of cell populations often consist of multiple modalities, e.g. a BF channel and a channel showing the nuclear staining and are named according to the dye used e.g. Hoechst (see Fig. 1). The latter channel (i.e. Hoechst) or a channel that measures labeled green fluorescent protein (GFP) with a nuclear marker are predominantly used in research for studying cell morphology and consequent feature quantification (e.g. the total number of segments detected) [1, 2]. However, if cell nuclei are fragmented due to apoptosis, each cell consists of multiple segments (fragmented nuclei), which cannot be assigned to each other by only using the information given in the Hoechst channel. An example is given in Fig. 1. The image on the top left shows the BF channel, the bottom left image shows the nuclear staining (Hoechst channel) and the images on the right show cases where stained nuclei cannot easily be recognized as fragmented nuclei belonging to one and the same or multiple cells.

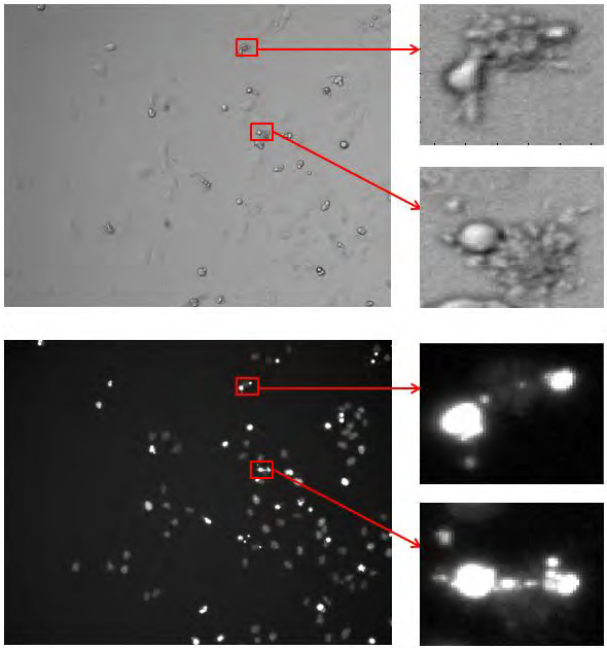

Figure 1: An example showing fragmented Hoechst segments in different channels : BF channel (top) and Hoechst channel (bottom) with problematic regions highlighted in red boxes (right side of each channel image) for both channels

The work done related to segmentation of cells with fragmented nuclei and segmentation in the BF channel can be seen in [3, 4, 5, 6]. However, combining multichannel information for the correct assignment of segments obtained from a single channel needs to be explored in more detail. Here, we propose a method to improve the segmentation process for fragmented segments. In cases where multiple neighboring nuclear fragments occur, cell shape features from the BF channel can be effectively used. This method includes information from both Hoechst and BF channels especially in cases where segments cannot be infallibly assigned. The BF channel exhibits distinctive features due to shadows arising from membrane blebbing or cellular protrusions. The main idea is to use the segments in the BF channel as a measure for cellular integrity and combine this information with the segments representing fragmented nuclei in the Hoechst channel.

2 Methods

The image processing pipeline implemented for this task is shown in Fig. 2. BF channel segment information is extracted by applying a Sobel edge detector to the BF channel image. The extracted segments are further processed sequentially using morphological operators i.e. image closing, hole-filling and image opening respectively (Fig. 3).
In the next step, binary large objects (BLOBs) detected by

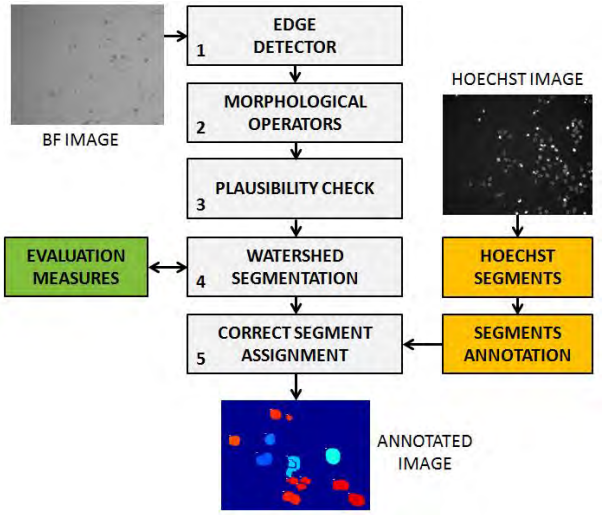

Figure 2: Complete image processing pipeline for assignment of Hoechst segments to their BF counterparts

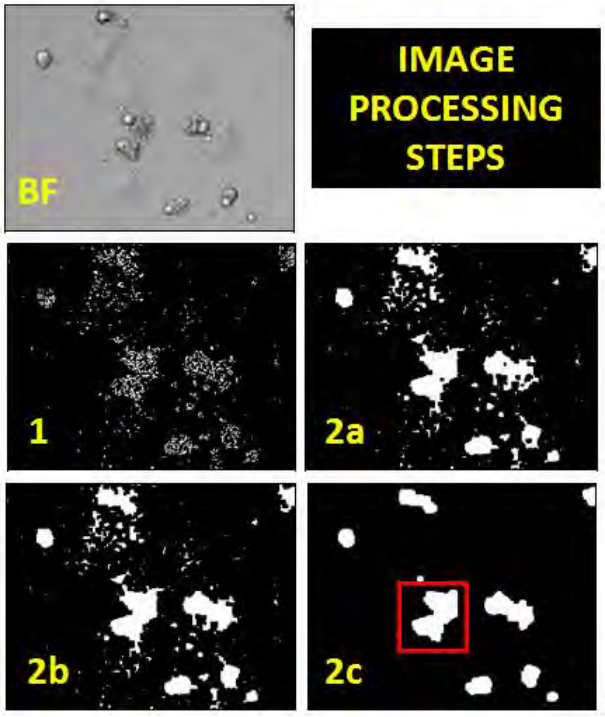

Figure 3: BF segmentation (steps 1-2 from Fig. 2): BF (section of original BF image), 1 (edge detector), 2a (image closing), 2b (hole filling) and 2c (image opening). Red box highlights an example of a potentially large BLOB according to plausibility criteria and therefore would be segmented further using step 4 in Fig. 2 i.e. watershed segmentation (see Fig. 4)

the operations 1-2 in Fig. 2 are further checked for plausibility (step 3 in Fig. 2). Criteria based on irregular size i.e. too small/big segments (approx. ranging from 200 to 1500 pixels) are implemented, thereby removing small objects and further segmenting big objects. A watershed segmentation seeking for gradients in brightness is known to perform well in cell separation [7, 8]. However, this separation cannot achieve the desired results due to inconsistencies caused by cellular fragmentation in both the channels. Therefore, we use the distance map of each BLOB. As a result all found BLOBs are within a given area range and show convex properties (see Fig. 4).

Figure 4: Watershed segmentation (see step 4 in Fig. 2) based on distance map: from left to right: BLOB (highlighted in red box in Fig. 3), distance map, separated objects

For Hoechst segmentation, we apply a segmentation routine described in [9, 10]. As a result we obtain $i = 1, ..., n$ segments in the BF channel and $j = 1, ..., m$ segments in the Hoechst channel. The pixel positions (x/y) belonging to the segments are gathered in the sets B_i for BF segments and D_j for Hoechst segments. The sets $D = \{D_1, ..., D_m\}$ and $B = \{B_1, ..., B_n\}$ define all found Hoechst and BF segments respectively.

If Hoechst segments belong to the same BF segment, they are annotated to the same class[1]. Therefore, the portion p_j of positive BF segment pixels in a Hoechst segment j is calculated and the most affecting BF segment is denoted as n_j (see Eq. 1,2 below).

$$p_j = \max_i \frac{\text{card}(D_j \bigcap B_i)}{\text{card}D_j}, \tag{1}$$

$$n_j = \arg\max_i \frac{\text{card}(D_j \bigcap B_i)}{\text{card}D_j}. \tag{2}$$

If $p_j \geq 0.1$, segment D_j is removed from the Hoechst segments and transferred to a set HOECHSTposBF segments DB. The set HOECHSTposBF contains segments in Hoechst which are also segmented in the BF channel. All segment sets being affected by the same BF segment are merged:

$$D = \{D_j | p_j < 0.1\}, \tag{3}$$

$$DB = \{DB_1, ..., DB_n\} \tag{4}$$

with

$$DB_i = \bigcup_{\substack{n_j = i \\ D_j >= 0.1}} D_j. \tag{5}$$

Empty sets in Eq. 4 are removed. All subsets in Eq. 3 denote BF-negative segments, all subsets in *DB* denote BF-positive segments. In this way segment reassignment is done (see step 5 in Fig. 2).

[1]If more than one BF segment affects the Hoechst segment, the most affecting BF segment will be chosen.

3 Results

The devised pipeline is applied to a biological dataset consisting of cis-platin treated human lung cancer cells (A549) acquired as described earlier [11]. This dataset contains some images of fragmented nuclei from cells that also show some distinctive features in the BF channel. Some images in this dataset contain 5 to 10 % of such cells. Therefore, room to improve the segmentation accuracy is evident. The results are shown in Fig. 5 and 6.

The goal of this processing pipeline is to annotate all segments correctly and assign only one label to all those nuclear segments that belong to one cell while giving each nucleus a unique label. All such segments belonging to each other are assigned the same number and exact same color in the final annotated image (a section of such an image is shown in Fig. 5). Here, the label 77 and specific red color tone is assigned to two segments that belong to each other. Therefore, it is easier for users to instantly see which segments belong to each other and vice versa.

Some *critical cases* using different channels separately and combined are shown in Fig. 6. *Critical cases* are those that require immediate assignment but were not obtained by using only Hoechst segments. The *critical cases* are a combination of:

1. fragmented nuclei (as defined by manual inspection) which however were labeled differently from each other using Hoechst segmentation only

2. oversegmentation of the nuclei thus generating a number of Hoechst segments not corresponding to the true number of nuclei

In Fig. 6, each column belongs to one of the several *critical cases*. The first row shows critical nuclear segments in the Hoechst channel and their corresponding appearance in the BF channel is given in the second row. The overlaid images are displayed in the third row and show the segments from Hoechst in red over the grayscale BF image. The resulting annotation shows segments that belong to each other encircled together in the final row. From Fig. 6, it is clear that with such a method *critical cases* can be resolved (also see Tab. 1).

However, the improvement in segmentation results is highly dependent upon the number of *critical cases* with respect to the total number of segments present in an image. If a higher number of fragmented nuclei belonging to the same cell is present, such an algorithm can highly improve the segmentation result (see Tab. 1).

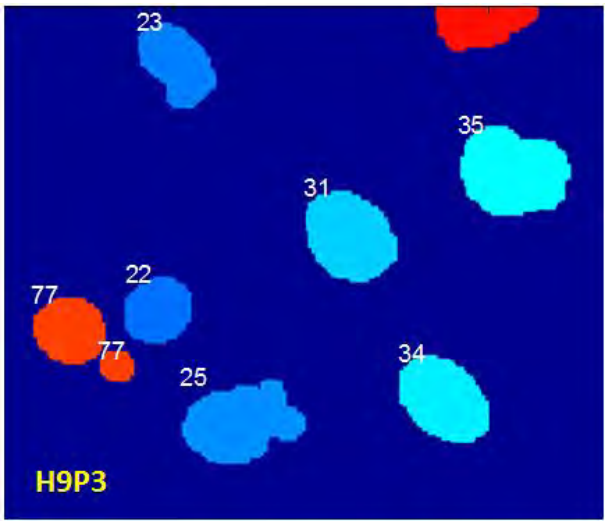

Figure 5: Output image annotated with colors and cell numbers

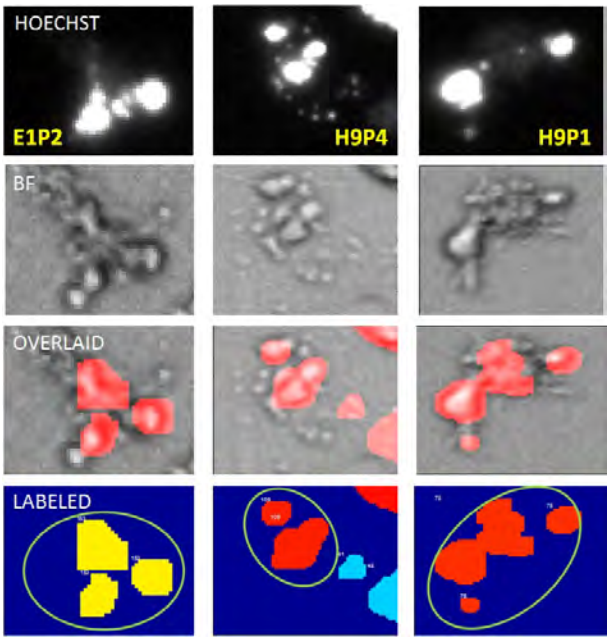

Figure 6: Solved *critical cases* from given dataset (1 case per column). The first row shows *critical cases* in the Hoechst channel. The second row shows the same *critical cases* in BF channel. The third row represents an overlay of the BF channel with the segments from the Hoechst channel (shown in red color). The final row represents annotated images whereby segments belonging to each other are encircled together (in green colored encirclements)

4 Conclusion and Outlook

This new method enables us to improve the nuclear segmentation outcome using morphological information from another channel thereby avoiding errors in counting fragmented nuclei. The number of fragmented nuclei would be underestimated in absence of such a method. In our next steps, the algorithm needs to be applied to a bigger dataset (including shading, noise etc.) to show robustness and performance improvement. Furthermore, implementation of automatic parameter tuning (as in big image processing pipelines) for optimization of such a method is required.

5 Acknowledgement

We express our gratitude to DAAD (German Academic Exchange Service) for funding this research work of A. Khan.

Table 1: Results of segment reassignment and segmentation improvement. The first column shows names of images containing *critical cases*. Some of these cases could be seen in Fig. 6. The second column shows the number of nuclear segments found using the Hoechst channel only. The third column shows the number of *critical cases* solved by using segmentation in the BF channel in addition to the already available Hoechst segmentation (e.g. the three *critical cases* shown in Fig. 6). Here, number of cases represents the total number of *critical cases* in a given image and number of segments represents the total number of segments that are involved in *critical cases*. The fourth column shows the total number of segments (belonging to *critical cases*) that are now assigned correctly using this methodology e.g., in column 1 and row 4 of Fig. 6 the two lower segments are now correctly assigned to the same cell shown within green encirclements. However, not in all *critical cases* the improved algorithm could correctly assign the segments as manual inspection revealed (listed in Tab. 1 as incorrect reassignment). The last column shows the improvement in segmentation results using this method. Here, the first sub-column is assigned to the % improvement in segmentation results using the total number of correct segments with respect to the total number of segments detected originally in a given image. This percentage is simply calculated using: 100 × (1 - (total Hoechst segments without using BF channel - difference of correct and incorrect number of segments after reassignment)) / total Hoechst segments without using BF channel. The second sub-column is dedicated to segmentation success with respect to the number of *critical cases* solved. This percentage is simply calculated as: 100 × (segments reassigned correctly - segments reassigned incorrectly) / total number of reassigned segments per image. **NOTE:** no. and w.r.t are the abbreviations for number and with respect to respectively.

	total segments	***critical cases***		**segments reassigned**		**segmentation correction (%)**	
Image name	*from Hoechst*	*no. of cases*	*no. of segments*	*correct*	*incorrect*	*w.r.t image*	*w.r.t critical cases*
E1P2	266	11	24	9	4	1.88	69.2
H1P3	82	1	2	1	0	1.22	100
H3P4	40	7	16	8	1	17.5	88.89
H8P4	88	4	9	5	0	5.80	100
H9P1	104	7	17	7	3	3.85	70
H9P4	138	5	11	5	1	2.90	83.3

6 References

[1] B. Neumann, T. Walter, J.-K. Hériché, J. Bulkescher, H. Erfle, C. Conrad, P. Rogers, I. Poser, M. Held, U. Liebel, *et al.*, "Phenotypic profiling of the human genome by time-lapse microscopy reveals cell division genes," *Nature*, vol. 464, no. 7289, pp. 721–727, 2010.

[2] J. Stegmaier, J. C. Otte, A. Kobitski, A. Bartschat, A. Garcia, G. U. Nienhaus, U. Straehle, and R. Mikut, "Fast segmentation of stained nuclei in terabyte-scale, time resolved 3d microscopy image stacks," *PLOS ONE*, vol. 9, no. 2, p. e90036, 2014.

[3] F. Buggenthin, C. Marr, M. Schwarzfischer, P. S. Hoppe, O. Hilsenbeck, T. Schroeder, and F. J. Theis, "An automatic method for robust and fast cell detection in bright field images from high-throughput microscopy," *BMC bioinformatics*, vol. 14, no. 1, p. 297, 2013.

[4] Z. Bacsó, R. B. Everson, and J. F. Eliason, "The DNA of annexin v-binding apoptotic cells is highly fragmented," *Cancer Research*, vol. 60, no. 16, pp. 4623–4628, 2000.

[5] S. Henery, T. George, B. Hall, D. Basiji, W. Ortyn, and P. Morrissey, "Quantitative image based apoptotic index measurement using multispectral imaging flow cytometry: A comparison with standard photometric methods," *Apoptosis*, vol. 13, no. 8, pp. 1054–1063, 2008.

[6] L. Galluzzi, S. A. Aaronson, J. Abrams, E. S. Alnemri, D. W. Andrews, E. H. Baehrecke, N. G. Bazan, M. V. Blagosklonny, K. Blomgren, C. Borner, *et al.*, "Guidelines for the use and interpretation of assays for monitoring cell death in higher eukaryotes," *Cell Death & Differentiation*, vol. 16, no. 8, pp. 1093–1107, 2009.

[7] S. Beucher and F. Meyer, *Mathematical Morphology in Image Processing*, ch. The morphological approach to segmentation: The watershed transformation., pp. 433–481. 1993.

[8] A. Pinidiyaarachchi and C. Wählby, "Seeded watersheds for combined segmentation and tracking of cells," in *Image Analysis and Processing–ICIAP 2005*, pp. 336–343, Springer, 2005.

[9] A. Khan, M. Reischl, B. Schweitzer, C. Weiss, and R. Mikut, "Feedback-driven design of normalization techniques for biological images using fuzzy formulation of a priori knowledge," *Studies in Computational Intelligence*, vol. 445, pp. 167–178, 2013.

[10] A. Khan, R. Mikut, B. Schweitzer, C. Weiss, and M. Reischl, "Automatic tuning of image segmentation parameters by means of fuzzy feature evaluation," *Advances in Intelligent Systems and Computing*, vol. 190, no. 5, pp. 459–467, 2013.

[11] J. Donauer, I. Schreck, U. Liebel, and C. Weiss, "Role and interaction of p53, bax and the stress-activated protein kinases p38 and jnk in benzo(a)pyrene-diolepoxide induced apoptosis in human colon carcinoma cells," *Archives of Toxicology*, vol. 86(2), pp. 329–337, 2012.